Molecular dynamics simulations of optical conductivity of dense plasmas

I. Morozov
Institute for High Energy Densities of RAS, IHED-IVTAN, Izhorskaya, 13/19, Moscow 127412, Russia

H. Reinholz, G. Röpke, and A. Wierling
University of Rostock, Institut für Physik, Universitätsplatz 3, D-18051 Rostock, Germany

G. Zwicknagel
University of Erlangen, Institut für Theoretische Physik, Staudtstrasse 7, D-91058 Germany
(Received 20 February 2005; revised manuscript received 6 April 2005; published 22 June 2005)

The optical conductivity $\sigma(\omega)$ for dense Coulomb systems is investigated using molecular dynamics simulations on the basis of pseudopotentials to mimic quantum effects. Starting from linear response theory, the response in the long-wavelength limit $k=0$ can be expressed by different types of autocorrelation functions (ACF's) such as the current ACF, the force ACF, or the charge density ACF. Consistent simulation data for transverse as well as longitudinal ACF's are shown which are based on calculations with high numerical accuracy. Results are compared with perturbation expansions which are restricted to small values of the plasma parameter. The relevance with respect to a quantum Coulomb plasma is discussed. Finally, results are presented showing a consistent description of these model plasmas in comparison to quantum statistical approaches and to experimental data.

DOI: 10.1103/PhysRevE.71.066408 PACS number(s): 52.65.Yy, 52.25.Mq, 71.45.Gm, 52.27.Gr

I. INTRODUCTION

In the present paper, we report molecular dynamics (MD) simulations to evaluate the transport properties of dense plasmas. We compare with quantum-statistical calculations and experimental results. To start with, some notations relevant for the introduction of the optical conductivity and the dynamical collision frequency are given.

The different optical and transport properties of Coulomb systems are related to the dielectric tensor $\hat{\epsilon}(\vec{k},\omega)$. The dynamical and static structure factor, optical spectra, bremsstrahlung, stopping power, reflectivity, dc conductivity, and other properties have been investigated recently [1–4]. For an isotropic and homogeneous system, the dielectric tensor can be decomposed into a longitudinal and a transverse part

$$\epsilon_{ij}(\vec{k},\omega)=\epsilon^{\mathrm{L}}(\vec{k},\omega)\frac{k_i k_j}{k^2}+\epsilon^{\mathrm{T}}(\vec{k},\omega)\left(\delta_{ij}-\frac{k_i k_j}{k^2}\right)=\begin{pmatrix}\epsilon^{\mathrm{T}} & 0 & 0\\ 0 & \epsilon^{\mathrm{T}} & 0\\ 0 & 0 & \epsilon^{\mathrm{L}}\end{pmatrix}, \tag{1}$$

where the matrix representation is valid assuming $\vec{k}=k\vec{e}_z$. The longitudinal part is related to the dynamical structure factor

$$S(\vec{k},\omega)=\frac{\epsilon_0 k^2}{ne^2}\frac{\hbar}{\mathrm{e}^{-\beta\hbar\omega}-1}\,\mathrm{Im}\,\frac{1}{\epsilon^{\mathrm{L}}(\vec{k},\omega)}, \tag{2}$$

which will be used as the starting point in the upcoming discussion. n denotes the charge density.

A related quantity is the nonlocal dynamical conductivity $\hat{\sigma}(\vec{k},\omega)$ which is defined according to $\hat{\epsilon}(\vec{k},\omega)=1+i\hat{\sigma}(\vec{k},\omega)/(\epsilon_0\omega)$ and can also be decomposed into a longitudinal $\sigma^{\mathrm{L}}(\vec{k},\omega)$ and transverse $\sigma^{\mathrm{T}}(\vec{k},\omega)$ part. In the long-wavelength limit ($k\to 0$), both longitudinal and transverse quantities coincide and lead to the same response of the system,

$$\sigma(\omega)=\lim_{k\to 0}\sigma^{\mathrm{T}}(\vec{k},\omega)=\lim_{k\to 0}\sigma^{\mathrm{L}}(\vec{k},\omega), \tag{3}$$

where $\sigma(\omega)$ is denoted as the optical (or dynamical) conductivity. For applications with respect to the optical properties of plasmas, this limit can be taken if the wavelength of the electromagnetic radiation is large compared to the distances of the charge separation. In particular, $\sigma(0)=\sigma_{\mathrm{dc}}$ describes the static dc conductivity. The dynamical conductivity is related to the dynamical collision frequency $\nu(\omega)$ via a generalized Drude formula [5,6]

$$\sigma(\omega)=\frac{\epsilon_0\omega_{\mathrm{pl}}^2}{-i\omega+\nu(\omega)}, \tag{4}$$

where $\omega_{\mathrm{pl}}=(\Sigma_c n_c e_c^2/\epsilon_0 m_c)^{1/2}$ is the plasma frequency with n_c being the particle density, e_c the charge, and m_c the mass of the component species c (note that spin is included as well). Thus, alternatively, the collision frequency can be considered as the quantity which contains all the information on microscopic processes in the system. The present paper is concerned with the investigation of $\sigma(\omega)$ or $\nu(\omega)$, respectively, and, in particular, the dc limit.

Starting from the microscopic description, we will consider a nonrelativistic two-component fully ionized neutral plasma, such as a H plasma consisting of electrons and ions (protons), at temperature T and density $n=n_{\mathrm{e}}=n_{\mathrm{i}}$ of each component. Within the Coulomb system, the coupling to a transverse vector potential is neglected, thus not accounting for radiative corrections. This is possible for temperatures

TABLE I. Parameters and results of MD simulations for the corrected Kelbg potential, Eq. (8), at $\Gamma=1$. The index number refers to different temperatures. The corresponding values for the electron density n_e and the degeneracy parameter Θ, and the interaction potentials at zero distance $V_{ei}(0)/k_BT$ and $V_{ee}(0)/k_BT$ are given; see also Fig. 1. For the collision frequency at zero frequency $\nu(0)$ and the $\alpha_{r/i}$ characterizing the high-frequency behavior of its real and imaginary part, see Sec. IV.

No.	T (10^3 K)	n_e (10^{21} cm^{-3})	Θ	$V_{ei}(0)/k_BT$	$V_{ee}(0)/k_BT$	$\nu(0)/\omega_{pl}$	α_r	α_i
1	16	0.2096	10.71	−8.52	7.49	0.224	3.4±0.3	1.05±0.06
2	33	1.839	5.20	−6.83	5.61	0.221	3.8±0.2	1.05±0.02
3	100	51.17	1.71	−4.49	3.64	0.150	3.5±0.4	1.04±0.02
4	350	2194	0.49	−2.49	2.31	0.032	3.4±0.7	1.02±0.04

not too high as considered here. The interactions are described by the longitudinal part, the Coulomb potential, and the Hamiltonian is

$$H=\sum_{c,\alpha}\frac{p_{c,\alpha}^2}{2m_c}+\frac{1}{2}\sum_{\{c,\alpha\}\neq\{d,\beta\}}\frac{e_ce_d}{4\pi\epsilon_0|\vec{r}_{c,\alpha}-\vec{r}_{d,\beta}|}, \tag{5}$$

with α, β denoting the index of the particle of components c, d, respectively. Thus, only longitudinal (plasmons), but no transverse (photons), excitations are described by the Coulomb Hamiltonian. In thermal equilibrium, the plasma is characterized by the coupling parameter $\Gamma=e^2(4\pi n/3)^{1/3}(4\pi\epsilon_0k_BT)^{-1}$ and the degeneracy parameter $\Theta=2m_ek_BT\hbar^{-2}(3\pi^2n)^{-2/3}$. Details of the plasma properties density, temperature, and degeneracy at $\Gamma=1$ relevant for our calculations are given in Table I. Besides the values given in the table, we consider parameters of density $n=3.8\times10^{21}$ cm^{-3} and temperature of $T=33\,000$ K which is motivated by recent experiments in dense xenon plasmas [4]. They correspond to a nondegenerate ($\Theta=3.2$) and strongly coupled plasma ($\Gamma=1.28$). Note that the conditions given in Table I actually correspond to partially ionized plasmas since the Debye screening length $r_D=(\Sigma_cn_ce_c^2/\epsilon_0k_BT)^{-1/2}$ is on the order of the Bohr radius. We consider only free charge carriers in the context of a partially ionized plasma; the bound electrons (atoms) are neglected. A comprehensive treatment of these systems should account for bound states as well; see Ref. [7] and Sec. VI.

We are interested in the reaction of the system to an external perturbation. In the case of weak external fields considered here, linear response theory can be applied. Strong external fields produced, e.g., in high-intense ultrashort laser pulses, lead to large quiver velocities of the electrons exceeding the range of linear response. Collisional absorption in strong electrical fields has been investigated by different authors; see, e.g., Refs. [8–11]. A comparison of our linear response treatment with the strong field case will be given at the end of Sec. IV.

Within linear response theory, transport coefficients, in particular the dynamical conductivity, and further quantities such as the dynamical collision frequency are related to equilibrium correlation functions. Analytical expressions have been derived in earlier papers [5,6,12] and have been evaluated within approximation schemes as outlined below. These quantum statistical approaches are limited to small coupling parameters—e.g., $\Gamma\ll1$. Simulations are necessary to check the range of validity of these approximations and to extend the range of parameter values. Classical MD simulations [1,13–17] calculate the trajectories of a finite number of particles, neglecting the quantum character of the dynamical evolution of the many-particle system. A quantum-statistical treatment can be given using wave packet molecular dynamics [18] or applying path integral techniques [19].

The use of classical MD simulations for the evaluation of static equilibrium properties, such as the equation of state, has been shown to be equivalent to a quantum treatment. For this, the original Coulomb interaction is replaced by an appropriate pseudopotential, where the short-range part of the interaction is modified, reflecting the quantum character of the interaction [20]. In particular, the singularity of the Coulomb potential at $r=0$ has to be smeared out to avoid instabilities. Potentials which are motivated in this way can also be used in other classical calculations—e.g., equilibrium correlation functions—as they are of interest with respect to transport and optical properties. For MD simulations of nonideal plasmas, the Deutsch interaction potential [21] was used in the pioneering works [13] and later simulations [22,23]. It has the form

$$V_{cd}^D(r)=\frac{e_ce_d}{4\pi\epsilon_0r}\left[1-\exp\left(-\frac{r}{\lambda_{cd}^D}\right)\right], \tag{6}$$

where the parameter

$$\lambda_{cd}^D=\frac{1}{\sqrt{\pi}}\lambda_{cd}=\frac{\hbar}{\sqrt{2\pi m_{cd}k_BT}},\quad \frac{1}{m_{cd}}=\frac{1}{m_c}+\frac{1}{m_d}, \tag{7}$$

is related to the thermal wavelength

$$\Lambda_{cd}=\sqrt{2\pi\hbar^2/(m_c+m_d)k_BT}$$

.

A more systematic derivation of a pseudopotential which reproduces the equilibrium properties of the quantum Coulomb system via classical statistics has been given by Kelbg-see [20,24]-on the basis of Slater sums. In particular, we use the so-called "corrected Kelbg" potential [25]

$$V_{cd}^K(r)=\frac{e_ce_d}{4\pi\epsilon_0r}\left[F\left(\frac{r}{\lambda_{cd}}\right)-r\frac{k_BT}{e_ce_d}\tilde{A}_{cd}(\xi_{cd})\exp\left(-\frac{r^2}{\lambda_{cd}^2}\right)\right], \tag{8}$$

with

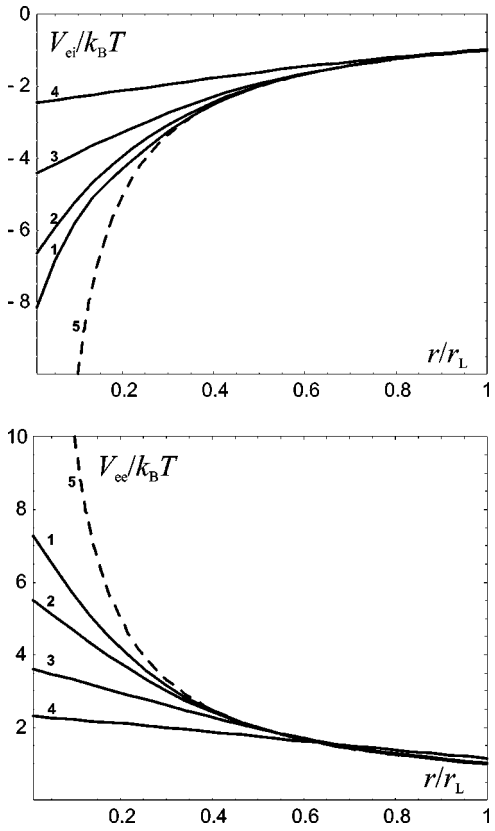

FIG. 1. Interaction potentials as function of distance, $r_L = e^2/(4\pi\varepsilon_0 k_B T)$: (left) electron-ion $V_{ei}(r)$, (right) electron-electron $V_{ee}(r)$; 1–4: Kelbg potential (8) at temperatures given by the corresponding index numbers in Table; I. 5: Coulomb potential.

$$\xi_{cd} = -\frac{e_c e_d}{k_B T \lambda_{cd}}, \quad F(x) = 1 - \exp(-x^2) + \sqrt{\pi}x[1 - \mathrm{erf}(x)],$$

$$\tilde{A}_{ee}(\xi_{ee}) = \sqrt{\pi}|\xi_{ee}| + \ln\left[2\sqrt{\pi}|\xi_{ee}|\int_0^\infty \frac{y\exp(-y^2)dy}{\exp(\pi|\xi_{ee}|/y) - 1}\right],$$

$$\tilde{A}_{ei}(\xi_{ei}) = -\sqrt{\pi}\xi_{ei} + \ln\left[\sqrt{\pi}\xi_{ei}^3\left(\zeta(3) + \frac{1}{4}\zeta(5)\xi_{ei}^2\right) + 4\sqrt{\pi}\xi_{ei}\int_0^\infty \frac{y\exp(-y^2)dy}{1 - \exp(-\pi\xi_{ei}/y)}\right],$$

where $\zeta(n)$ is the Riemann-Zeta function. Note that the definition of the parameter λ_{cd}, Eq. (7), is slightly different from λ_{cd}^D for the Deutsch potential. The interaction potential (8) corresponds to the Coulomb potential at large distances and provides an exact value of the Slater sum and its first derivative at $r=0$. Figure 1 shows the pseudopotential for the parameters given in Table I which will be used in the calculations and simulations later on. The temperature determines the depth of the short-range part in the corrected Kelbg potential. Further columns refer to the dynamical collision frequency and will be explained below; see Sec. IV.

Our aim is to compare different approaches to the dynamical conductivity of dense plasmas. Classical MD simulations based on an appropriate pseudopotential are compared with the analytical quantum treatment of the Coulomb system. This allows us to discuss the justification of the application of pseudopotentials in numerical simulations; see Sec. IV. Both approaches are discussed in the context of experimental data, in particular the static conductivity of fully ionized dense plasmas.

II. DYNAMICAL STRUCTURE FACTOR AT FINITE WAVE NUMBER

Within linear response theory, the response to external perturbations is given in terms of equilibrium correlation functions according to the fluctuation-dissipation theorem [14,20,26–28]; see also [29]. In the following, we consider the dynamical structure factor (2) which is a typical quantity in classical MD simulations. It is given by [14]

$$S(\vec{k},\omega) = \frac{1}{2\pi N}\int \mathrm{d}t \int \mathrm{d}^3 r \int \mathrm{d}^3 r' \langle \rho(\vec{r},t)\rho(\vec{r}',0)\rangle \mathrm{e}^{i\vec{k}\cdot(\vec{r}-\vec{r}')-i\omega t} \tag{9}$$

$$= \frac{1}{2\pi N}\int \mathrm{d}t \, \langle \rho_k(t)\rho_k^*(0)\rangle \mathrm{e}^{-i\omega t}, \tag{10}$$

where $\rho_k(t)$ is the Fourier transform of the charge density $\rho(\vec{r},t) = \Sigma_{c,\alpha} e_c \delta(\vec{r} - \vec{r}_{c,\alpha}(t))$. The angular brackets denote an average over the thermodynamic equilibrium distribution and define the correlation function

$$K_{AB}(t) = \langle A(t)B\rangle = \lim_{T\to\infty}\frac{1}{T}\int_{t_0}^{t_0+T} \mathrm{d}t' A(t+t')B(t'). \tag{11}$$

Corresponding to the principle of ergodicity, it is assumed that the long-time behavior of a trajectory gives the ensemble average with respect to equilibrium. After some initial time to establish the equilibrium distribution in the system and to form the correlations using a special procedure described in [16], different pieces of a trajectory starting at t_0 can be taken to mimic the average over the thermal equilibrium. As shown in [17], these pieces are statistically independent if they are taken at times t_0 separated by at least the dynamical memory time.

The trajectories $\vec{r}_{c,\alpha}(t)$ are simulated by MD methods using periodic boundary conditions and the minimum image convention (see, e.g., [30]). The basic MD box has the edge size $L = (N/n)^{1/3}$ which is determined by the number of particles, N, in the basic cell at a given mean plasma density n. The images of this basic cell are generated by shifting the basic cell by integer multiples of L in all directions. The number of particles in our simulations ranges from $N = 200$ to 1000. The choice of N is dictated by the criterion that the screening length should be considerable smaller than the MD box size. Thus, for smaller Γ a larger simulation box is needed.

The forces $\vec{F}_{c,\alpha} = \vec{F}_{c,\alpha}^{\mathrm{short}} + \vec{F}_{c,\alpha}^{\mathrm{long}}$ on the particle labeled by α of species c due to the surrounding particles are separated

into two contributions. The short-range contribution $\vec{F}_{c,\alpha}^{\text{short}} = \Sigma'_{d,\beta} \vec{F}_{cd}(\vec{r}_{d,\beta}^{\text{NN}} - \vec{r}_{c,\alpha})$ is due to the nearest images (nearest neighbors) $\{d,\beta\} \neq \{c,\alpha\}$ of all the particles following the conventional MD techniques. The contribution $\vec{F}_{c,\alpha}^{\text{long}}$ originates from interactions with particles and images outside a basic cell centered around the position $\vec{r}_{c,\alpha}$ of the particle $\{c,\alpha\}$. Part of the influence of these far images can be approximately taken into account considering Ewald sums [13,14]. As will be shown below, if the dimension L of the basic cell is large in comparison to the screening length, the contribution of the Ewald sums turns out to be small.

Another feature of long-range interactions is determined by the mean electrical field which is produced from the charge separation at scales larger than L according to the Maxwell equations. In particular, we are interested in plasmon excitations. Considering macroscopic charge density waves $\overline{\rho_k}(t) = \int d^3r \langle \rho(\vec{r},t) \rangle \exp(i\vec{k}\cdot\vec{r})$ with wave vector $\vec{k} = k\vec{e}_z$ [we have already assumed in Eq. (1) that they are propagating in z direction], we obtain a long-range mean field $\overline{E_k^z}(t) = \int d^3r E^z(\vec{r},t) \exp(i\vec{k}\cdot\vec{r})$ according to the Gauss law as

$$ik\overline{E_k^z}(t) = \frac{1}{\epsilon_0}\overline{\rho_k}(t). \tag{12}$$

This mean field produces a force on the charges so that they are accelerated. This results in a change of the average macroscopic current,

$$J_k^z(t) = \langle j_k^z(t) \rangle = \int d^3r \, \langle j^z(\vec{r},t) \rangle \exp(i\vec{k}\cdot\vec{r}), \tag{13}$$

with the longitudinal component of the current density:

$$\vec{j}(\vec{r},t) = \sum_{c,\alpha} e_c \, \vec{v}_{c,\alpha}(t) \, \delta(\vec{r} - \vec{r}_{c,\alpha}(t)). \tag{14}$$

The current density is related to the time variation of the charge density according to the balance equation $d\overline{\rho_k}(t)/dt = -ikJ_k^z(t)$, and plasma oscillations are obtained. We will demonstrate this in detail for the special case $k=0$ in the following section.

Since this mean field is long ranged and not restricted to the screening length, it has to be taken into account adequately and should not be influenced by the size L of the periodic boxes. Therefore, the dynamical structure factor can only be calculated for $k \geqslant 2\pi/L$. Only in this case, the density fluctuations which lead to plasmon oscillations correctly treated considering all particles within the basic MD box. Plasma waves with wavelengths exceeding the length L of the basic box are not correctly implemented by using periodic boundary conditions. Consequently, it is not possible in this way to describe collective excitations in the limit $k \to 0$.

Calculations of the dynamical structure factor at $k \geqslant 2\pi/L$ have been performed for the system considered here; see [1]. It has been shown that for $\Gamma \leqslant 2$ the MD simulations for the dynamical structure factor at finite values of k are in good agreement with the analytical results obtained within perturbation theory [1,31]. In particular, the plasmon peak is well reproduced. However, no results for the response to a homogeneous external field, $k=0$, can be obtained within this approach.

III. CURRENT AUTOCORRELATION FUNCTION AT ZERO WAVE NUMBER

As discussed above, it is impossible to carry out the long-wavelength limit $k \to 0$ in calculating the dynamical structure factor from the charge autocorrelation function (ACF), because of the finite extension of the MD basic simulation box. However, it is possible to consider this limit for the current ACF, as will be argued now. In the current ACF, plasmon oscillations will appear in the limit $k \to 0$ as well. Charge separation at long distances produces a surface charge density. If the surface is far away, it produces a homogeneous ($k=0$) mean electrical field within the simulation box which is necessary to include in the long-wavelength limit. As a consequence, plasma oscillations are obtained.

On the macroscopic level, the Maxwell equations relate this mean field to the z component of the average current density. Following Eq. (12) and the discussion in the previous section, we find in the Fourier space

$$\frac{d}{dt}\overline{E_{k=0}^z}(t) = -\frac{1}{\epsilon_0} J^z(t), \tag{15}$$

with the macroscopic current

$$\vec{J}_{k=0}(t) = \vec{J}(t) = \langle \vec{j}(t) \rangle = \left\langle \sum_{c,\alpha} e_c \vec{v}_{c,\alpha}(t) \right\rangle \tag{16}$$

as an average over the basic simulation cell. Taking the initial condition $\vec{E}(0) = 0$, the integration of Eq. (15) leads to

$$E^z(t) = \frac{1}{L^3}\overline{E_{k=0}^z}(t) = \frac{1}{\epsilon_0 L^3}\left\langle \sum_{c,\alpha} e_c r_{c,\alpha}^z(t) \right\rangle. \tag{17}$$

Neglecting the contribution from the Ewald sums, the long-range interaction forces are given by the mean field according to $\vec{F}_{c,\alpha}^{\text{long}}(t) = e_c E^z(t) \vec{e}_z$ which contribute to the longitudinal component. In particular, the equation of motion for an electron reads

$$m_e \frac{d\vec{v}_{e,\alpha}}{dt} = \vec{F}_{e,\alpha}^{\text{short}} - eE^z(t)\vec{e}_z. \tag{18}$$

The short-range forces $\vec{F}_{e,\alpha}^{\text{short}}$ are fluctuating around a zero mean value. But the amplitude of these fluctuations is much larger than the fluctuations of the mean-field force $-eE^z(t)\vec{e}_z$. It has been shown that the energy is conserved if the associated energy of the mean field is included [12].

The occurrence of plasma oscillations can be demonstrated in the following way. If the mass ratio between electrons and ions m_e/m_i is small, the ion current can be neglected. The derivative of the averaged total current density is obtained as

$$\frac{d}{dt}\vec{J}(t) = -e\left\langle \sum_{\alpha=1}^{N} \frac{d}{dt}\vec{v}_{e,\alpha} \right\rangle = \frac{eN}{m_e}[eE^z(t)\vec{e}_z - \langle \vec{\xi} \rangle], \tag{19}$$

$$\vec{\xi} = \frac{1}{N}\sum_{\alpha=1}^{N} \vec{F}_{e,\alpha}^{\text{short}} = \frac{1}{N}\sum_{\alpha=1}^{N}{\sum_{i,\beta}}' \vec{F}_{ei}(\vec{r}_{i,\beta}^{\text{NN}} - \vec{r}_{e,\alpha}). \quad (20)$$

The force $\vec{\xi}$ includes only electron-ion interaction forces. All electron-electron interaction forces are compensated since they do not change the total momentum of the electrons. Although the force $\vec{F}_{e,\alpha}^{\text{short}}$ on each electron is typically much greater than the force $eE^z(t)\vec{e}_z$ from the polarization field, the average over all electrons is of the same order of magnitude as $eE^z(t)$. If we now differentiate Eq. (15) and substitute the derivative of the current using Eq. (19), we obtain the equation for the mean field:

$$\frac{d^2}{dt^2}E^z(t) + \omega_{\text{pl}}^2 E^z(t) = \frac{\omega_{\text{pl}}^2}{e}\langle \xi^z \rangle. \quad (21)$$

In the average, $\langle \vec{\xi} \rangle$ vanishes, so that plasma oscillations are described. The corresponding oscillations in the current ACF as obtained from MD simulations are shown below.

Due to the mean field, MD simulations for the z direction [longitudinal component $j^{\text{L}}(t)$] and the x,y directions [transverse components $j^{\text{T}}(t)$] behave in different ways. In particular, two different current ACF's can be derived: the longitudinal one K_{jj}^{L} and the transverse one K_{jj}^{T}. Both were calculated separately in an earlier paper [12], using different MD simulation procedures, but can be derived from the same MD simulation if different components are taken. Within MD simulations [14,15], the normalized current ACF

$$K_{jj}^{\text{L/T}}(t) = \frac{\langle j^{\text{L/T}}(t) j^{\text{L/T}}(0)\rangle}{\langle j^2 \rangle} = \frac{\beta}{\epsilon_0 \omega_{\text{pl}}^2 L^3}\langle j^{z/x}(t) j^{z/x}(0)\rangle \quad (22)$$

is calculated. Here, the long-wavelength limit ($k \to 0$) of the Fourier transform (16) of the current density, Eq. (14), is considered, and the normalizing factor is equal to $\langle j^2 \rangle = e^2 N \langle v^2 \rangle / 3 = \epsilon_0 \omega_{\text{pl}}^2 L^3 / \beta$.

Using the balance equation $d\rho_k(t)/dt = -ikj_k^z(t)$ we can express the dynamical structure factor in terms of the longitudinal current ACF instead in terms of the density autocorrelation function (10). This ACF has been evaluated within MD simulations, solving the equation of motion and considering the z component of the current density. After implementing the mean field explicitly, the zero-wavelength limit can be considered. A detailed description of the MD simulation procedures is given in [31]. In particular, no dependence on the mass ratio for $m_e/m_i \leqslant 0.01$ was found.

As an illustration, we show results of MD simulations for the longitudinal and transverse current ACF in Fig. 2; see also [12]. It can be seen that after inclusion of a mean field acting on the z component, the plasma oscillations in $K_{JJ}^L(t)$ become well pronounced in contrast to a monotonously decreasing behavior for the correlation function K_{JJ}^T of the transverse current as was also obtained in previous MD simulations [13,15,17]. It should be stressed that the amplitude of the oscillations in the longitudinal case does not depend on the number of particles, N, in the simulation. The oscillation frequency tends to ω_{pl} for an ideal plasma [collision frequency $\nu(\omega) = 0$].

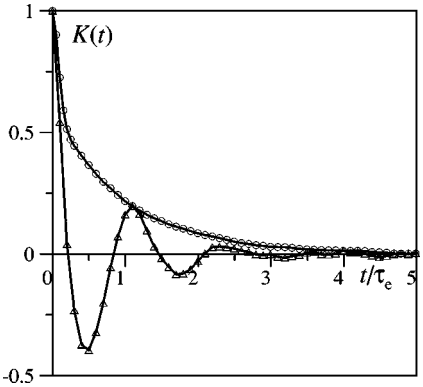

FIG. 2. Current autocorrelation function (22) for the Kelbg potential (8), $\Gamma = 1.28$, $m_e/m_i = 0.01$; total number of averages 5×10^5; MD trajectory length of $2.5 \times 10^4 \tau_e$, $\tau_e = 2\pi/\omega_{\text{pl}}$, period of electron plasma oscillations; circles, MD simulations $K_{JJ}^T(t)$ of components not influenced by the mean field, triangles, MD simulations $K_{JJ}^L(t)$ for the longitudinal component including the mean-field term in the equation of motion.

As a technical note, we mention that the contribution from the Ewald sums can be neglected for the parameter values considered here. This is expected for a nonideal plasma where the effective interaction potential decreases exponentially with distance due to screening. We illustrate this fact by comparing MD simulations with and without Ewald summations. The current ACF for a plasma at $\Gamma = 1$ and temperature of 316 000 K using the Deutsch potential is shown in Fig. 3. As can be seen, the neglect of Ewald sums is of no significance for the evaluation of these quantities. This is also found for the dynamical collision frequency discussed below, which is shown for these particular MD simulations without and including Ewald sums in Fig. 4.

IV. DYNAMICAL COLLISION FREQUENCY

We will now discuss the results of the current ACF in the context of the dynamical conductivity and the dynamical collision frequency. Within linear response theory, the current

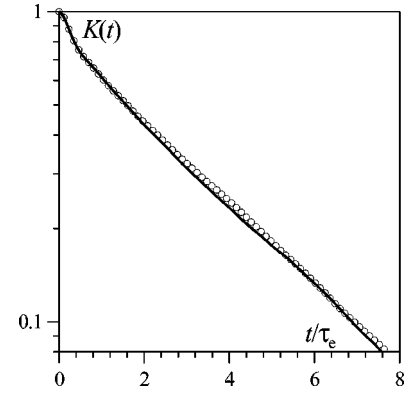

FIG. 3. Results of MD simulations with the Deutsch potential (6) for the transverse current ACF (22) using nearest image method without Ewald sums (circles) and simulations including Ewald sums (solid line) for $\Gamma = 1$, $T = 316\,000$ K.

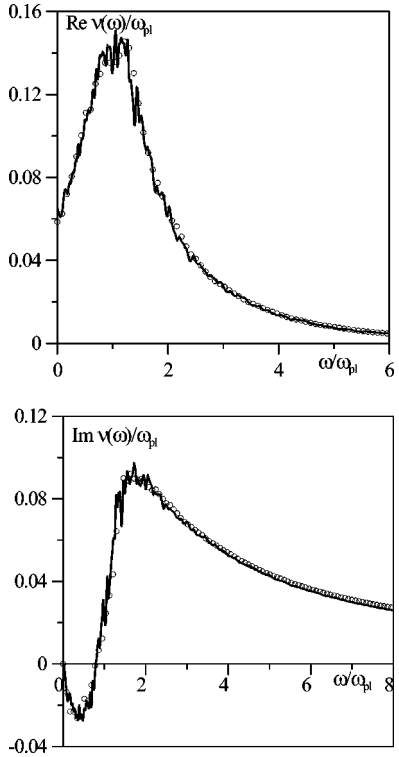

FIG. 4. Comparison of dynamical collision frequency, determined from MD simulations via the minimum image method without Ewald sums (circles) and simulations including Ewald sums (solid line) for $\Gamma=1$, $T=316\,000$ K, using the Deutsch potential (6).

ACF can be related to the longitudinal and transverse conductivity, respectively. According to [12], we find for the longitudinal case

$$\sigma^{\mathrm{L}}(k,\omega)=\frac{(\beta/L^3)\langle j_k^{\mathrm{L}};j_k^{\mathrm{L}}\rangle_{\omega+i\eta}}{1-(i\beta/\epsilon_0\omega L^3)\langle j_k^{\mathrm{L}};j_k^{\mathrm{L}}\rangle_{\omega+i\eta}} \tag{23}$$

and the transverse case

$$\sigma^{\mathrm{T}}(k,\omega)=\frac{\beta}{L^3}\langle j_k^{\mathrm{T}};j_k^{\mathrm{T}}\rangle_{\omega+i\eta}\,, \tag{24}$$

where the correlation function $\langle A;B\rangle_{\omega+i\eta}=\int_0^\infty \mathrm{e}^{i(\omega+i\eta)t}\langle A(t)B(0)\rangle \mathrm{d}t$ is the Laplace transform of the respective ACF. The limit $\eta\to 0$ has to be taken after the thermodynamic limit.

The longitudinal and transverse currents $j_k^{\mathrm{L/T}}(t)$ and their long-wavelength limit are given by the z component and x,y component, respectively, of the Fourier transform of the current density, Eqs. (14) and (16). Within a Green function approach to these correlation functions, a diagram representation is possible [5]. Since the coupling to the transverse vector potential is not considered, there are no reducible diagrams with respect to the transverse interaction and no term in the denominator as in the longitudinal case appears. Thus, the Kubo-Greenwood formula (24) [13–15,26–28] relates the dynamical conductivity directly to the transverse current ACF.

In the long-wavelength limit, the structure of the generalized Drude formula (4) is obtained. From this, the dynamical collision frequencies $\nu^{\mathrm{L/T}}(\omega)$ could be deduced, from either the longitudinal case or the transverse case, respectively,

$$\lim_{k\to 0}\sigma^{\mathrm{L/T}}(\vec{k},\omega)=\frac{\epsilon_0\omega_{\mathrm{pl}}^2}{-i\omega+\nu^{\mathrm{L/T}}(\omega)}. \tag{25}$$

Since the expressions between the conductivities and current-current correlation functions are different for the longitudinal and transverse cases, the deduced collision frequencies $\nu^{\mathrm{L}}(\omega)$ and $\nu^{\mathrm{T}}(\omega)$ are with Eqs. (23) and (24), respectively,

$$\frac{\nu^{\mathrm{L}}(\omega)}{\omega_{\mathrm{pl}}}=\frac{\epsilon_0\omega_{\mathrm{pl}}L^3}{\beta\langle j^{\mathrm{L}};j^{\mathrm{L}}\rangle_{\omega+i\eta}}+i\left(\frac{\omega}{\omega_{\mathrm{pl}}}-\frac{\omega_{\mathrm{pl}}}{\omega}\right), \tag{26}$$

$$\frac{\nu^{\mathrm{T}}(\omega)}{\omega_{\mathrm{pl}}}=\frac{\epsilon_0\omega_{\mathrm{pl}}L^3}{\beta\langle j^{\mathrm{T}};j^{\mathrm{T}}\rangle_{\omega+i\eta}}+i\frac{\omega}{\omega_{\mathrm{pl}}}. \tag{27}$$

The collision frequencies should be identical for $k\to 0$ since the dynamical conductivity is given according to Eqs. (3) and (4). However, the correlation functions are calculated with different schemes as explained before. The current correlation functions in the long-wavelength limit are given as

$$\langle j;j\rangle_{\omega+i\eta}=\langle j^2\rangle\int_0^\infty \mathrm{e}^{i(\omega+i\eta)t}K_{jj}(t)\mathrm{d}t. \tag{28}$$

The dynamical collision frequencies $\nu^{\mathrm{L/T}}(\omega)$ have been calculated from the simulation data for the current ACF's at zero wave number (see Fig. 2) and are shown in Fig. 5. Both coincide quite clearly as expected. Note the considerable improvement of accuracy in comparison to earlier results in Ref. [12]. Additional verification of self-consistency is performed by calculating Im $\nu(\omega)$ from Re $\nu(\omega)$ in accordance with the Kramers-Kronig rule. Therefore, our analysis showed that the transverse conductivity is identical with the longitudinal conductivity in the long-wavelength limit if the mean field is taken into account in the longitudinal case. This agreement and the validity of the Kramers-Kronig rule prove the high accurracy of our present MD simulations.

Instead of the current ACF, other correlation functions can be taken as well, in particular the force ACF or the current-force correlation function. The following relations could be used for this purpose:

$$\langle\vec{j};\vec{j}\rangle_\omega=\frac{i}{\omega}\left(\langle\vec{j}^2\rangle-\left\langle\vec{j};\frac{d}{dt}\vec{j}\right\rangle_\omega\right)=\frac{i}{\omega}\left(\langle\vec{j}^2\rangle-\frac{i}{\omega}\left\langle\frac{d}{dt}\vec{j};\frac{d}{dt}\vec{j}\right\rangle_\omega\right), \tag{29}$$

$$\frac{d}{dt}\vec{j}(t)=\sum_{c,\alpha}e_c\frac{d}{dt}\vec{v}_{c,\alpha}(t)=-e\left(\frac{1}{m_{\mathrm{e}}}+\frac{1}{m_{\mathrm{i}}}\right)\vec{F}_{\mathrm{e}}, \tag{30}$$

where $\vec{F}_{\mathrm{e}}=\Sigma_\alpha^N\vec{F}_{\mathrm{e},\alpha}$ stands for the resultant force of all ions on electrons as all internal forces between electrons as well as between ions cancel after summation.

Practically, the current ACF provides more accurate results for the low frequencies $\omega<\omega_{\mathrm{pl}}$ while the force ACF works better for high frequencies. Due to the finite numerical

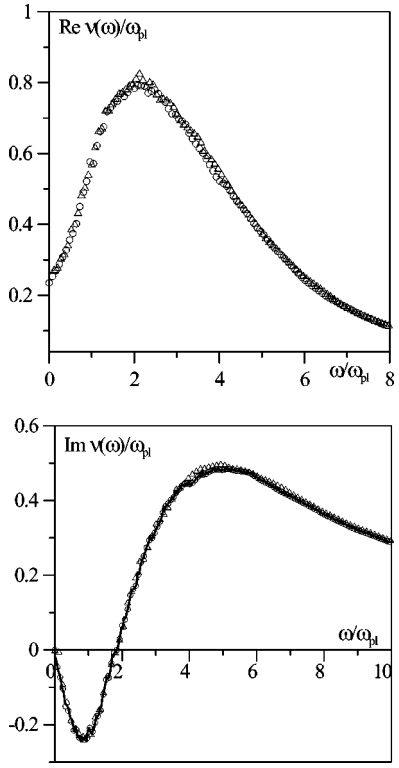

FIG. 5. Real and imaginary parts of the dynamic collision frequency from MD simulations for the Kelbg potential (8) in the long-wavelength limit of the transverse case (circles) and the longitudinal case (triangles), parameters as in Fig. 2; solid line-imaginary part obtained from the real part (transverse case) according to Kramers-Kronig rule. $T=33\,000$ K, $\Gamma=1.28$.

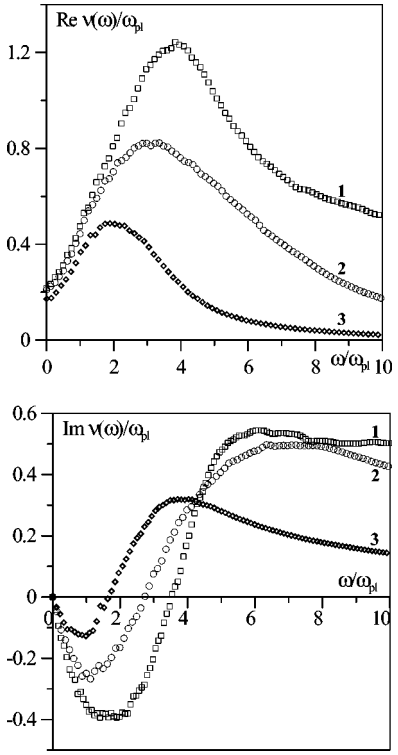

FIG. 6. Real and imaginary parts of the effective collision frequency for the Kelbg potential (8) at $\Gamma=1$ in dependence on temperature: 1: $T=16\,000$ K, 2: $T=33\,000$ K, 3: $T=80\,000$ K.

accuracy of the current ACF obtained from MD simulations, the linear term proportional to $i\omega$ in Eqs. (26) and (27) may lead to a divergent behavior of Im $\nu(\omega)\sim\omega$ at high frequencies. On the other hand, the corresponding relation for the force ACF has no such defect:

$$\nu^L(\omega)=\frac{i\omega\left\langle \frac{d}{dt}j^L;\frac{d}{dt}j^L\right\rangle_\omega}{i\epsilon_0\omega\omega_{\rm pl}^2L^3/\beta+\left\langle \frac{d}{dt}j^L;\frac{d}{dt}j^L\right\rangle_\omega}. \tag{31}$$

The real and imaginary parts of the dynamic collision frequency are presented in Fig. 6 for different temperatures at a coupling strength of $\Gamma=1$. Table I shows the parameters for the simulations in more details. It is seen that with decreasing temperature, the absolute values of the real and imaginary parts of the collision frequency increase over the whole frequency range. This is expected from Fig. 1, where the strength of the attractive potential increases also with decreasing temperature. Note that the peak in the real part is more pronounced and shifted to higher frequencies with decreasing temperature. Since the collision frequency is shown as a ratio with respect to the plasma frequency which decreases with decreasing temperature for a fixed Γ, this tendency is slightly suppressed in the presentation.

An important question is to which extent the MD simulations shown here are relevant for real Coulomb systems. The Kelbg potential was constructed to reproduce the static equilibrium properties of dense plasmas, and we expect that it should be appropriate at least to describe low-frequency, quasistatic properties. This assumption-whether classical simulations based on a pseudopotential can be used to mimic time-dependent properties of dense plasmas-can be checked by comparison with quantum statistical calculations

We will only briefly refer to the quantum statistical treatment of Coulomb systems. Details of different perturbative approximations for the dynamical collision frequency can be found in [5]. In particular, expressions for the collision frequency in the form of

$$\nu(\omega)=r(\omega)\nu^{(P_0)}(\omega) \tag{32}$$

have been given where $\nu^{(P_0)}(\omega)$ contains the contribution of the force-force correlation function in screened binary collision approximation and the renormalization factor $r(\omega)$ accounts for higher moments of the distribution function in calculating the response to external perturbations; see also [6]. As well known from the Chapman-Enskog approach in kinetic theory, higher moments of the distribution function have to be accounted for to include the effect of e-e collisions and to obtain the correct prefactor of the Spitzer result for the conductivity. The comparison of MD simulations with an analytical treatment is shown in Fig. 7. For this, strong collisions and dynamical screening are accounted for in a consistent manner by a Gould-DeWitt scheme for

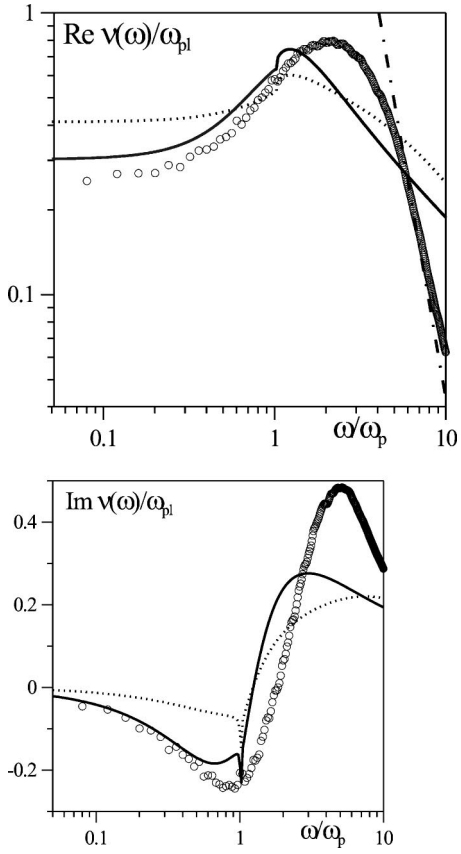

FIG. 7. Comparison between MD data for the Kelbg potential (8) (open circles) and the quantum-statistical treatment for the Coulomb potential. The Gould-DeWitt scheme is used, accounting for dynamical screening and strong binary collisions. Solid line: including the renormalization factor $r(\omega)$, Eq. (32). Dotted line: without the renormalization factor. The dot-dashed line gives the analytical result for the high-frequency behavior of Re $\nu(\omega)$ for the Kelbg potential (8). $\Gamma=1$, $T=33\,000$ K.

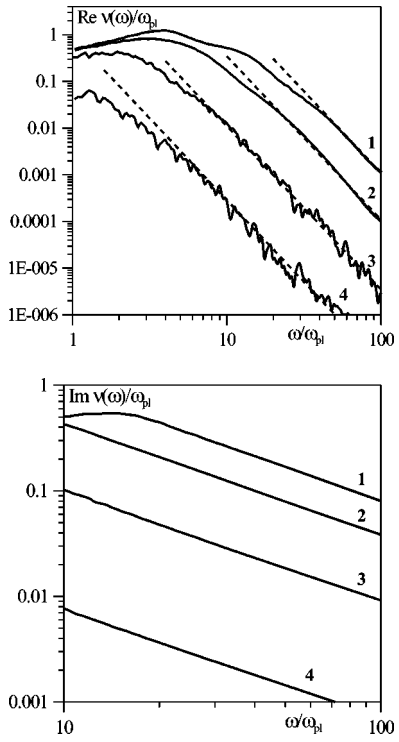

FIG. 8. Real and imaginary parts of the effective collision frequency at high frequencies with power fits for the Kelbg potential (8). Parameters correspond to the index numbers given in Table I. Dashed lines are the power-law fits Re $\nu\sim\omega^{-3.5}$. $\Gamma=1$.

$\nu^{(P_0)}(\omega)$. Furthermore, two moments are taken into account by a frequency-dependent renormalization factor $r(\omega)$ [5] which are evaluated in statically screened Born approximation. Good agreement for both the real and imaginary parts is observed for $\omega<\omega_{\rm pl}$; see [12]. In this region, the quantum-mechanical treatment of the Coulomb potential and the classical simulations based on the corrected Kelbg potential are consistent. Note that an evaluation of the force-force correlation function alone is not sufficient, and the renormalization factor has to be taken into account to obtain correct results, in particular in the low-density low-frequency limit.

In the high-frequency limit, the asymptotic behavior of the collision frequency for a Coulomb potential and a Kelbg potential differs. As a consequence, the agreement is poor for $\omega\geqslant\omega_{\rm pl}$. In order to investigate the high-frequency behavior of the simulation data in more detail, a logarithmic scaling is used in Fig. 8. The real part can be fitted by a power law Re $\nu(\omega)\sim\omega^{-\alpha_r}$. The corresponding values of α_r deduced from the simulation data are shown in Table I. The result is in good agreement with the analytical behavior of $\sim\omega^{-3.5}$ [32] for the Kelbg potential. However, it is in disagreement with the results for a Coulomb potential which gives $\sim\omega^{-1.5}$ in the high-frequency limit. Therefore, we conclude that the Kelbg pseudopotential is not able to correctly describe the high-frequency behavior of a Coulomb system. However, the imaginary part of the collision frequency follows the power law Im $\nu(\omega)\sim\omega^{-\alpha_i}$ with the exponent α_i deduced from the simulation data close to unity (see Table I), which is in agreement with the analytical result $\sim\omega^{-1}$, valid for both the Coulomb and Kelbg potentials.

In an earlier paper [33], a comparison of our perturbative approach to results obtained from a MD code by Pfalzner and Gibbon [34] has been reported for $\Gamma=0.1$. The collision frequency is derived from a heating rate using the high-frequency asymptote of the Drude formula. In this case, good agreement between MD simulations and analytical calculations for a classical model plasma is found for higher frequencies.

Figure 9 shows the comparison of MD simulations and perturbative results with Schlanges *et al.* [35] for a fixed density of $n=10^{22}$ cm^{-3} and frequency of $\omega=3\omega_{\rm pl}$ as a function of the coupling parameter Γ. Schlanges *et al.* considered strong fields, which are parametrized via a finite quiver velocity. With decreasing quiver velocity, the limit of linear response is approached [11,36]. Here, we consider a quiver velocity of $v=0.2v_{\rm th}$ which is given in terms of the thermal velocity $v_{\rm th}$ and is low enough to be already in the linear response regime. We find identical results if we evaluate the collision frequency (32) in the dynamically screened Born approximation (Lenard-Balescu collision term); see [5,6]. Dynamical screening within the Born approximation was also taken into account in Ref. [35]. On the other hand, MD

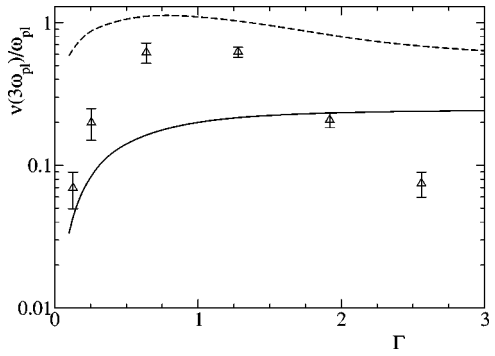

FIG. 9. Real part of the collision frequency for charge density $n_e = 10^{22}$ cm^{-3} at frequency $\omega = 3\omega_{\rm pl}$. Δ: MD results for the Kelbg potential (8). Solid curve: Ref. [35] for quiver velocity $v_0 = 0.2 v_{\rm th}$ as well as linear response on the level of dynamically screened Born approximation (Lenard-Balescu collision term). Dashed curve: linear response including strong collisions (T matrix).

simulations give results which are significantly higher than the results shown in Ref. [35]. The MD results for the dynamical collision frequency are, however, in qualitative agreement with the Gould-DeWitt result. Strong collisions are of relevance in this region. To support this, we show the result for the collision frequency calculated with the T-matrix collision term. We find significant differences between results for the collision frequency when taking into account beyond the static Born approximation either the effects of strong collisions or dynamical screening. In agreement with the treatment of the dynamical structure factor [1], the perturbative approach becomes invalid if Γ exceeds the value of about 2. As already seen from Fig. 7, an exact coincidence between MD simulations for the collision frequency based on the Kelbg pseudopotential (or other forms of the pseudopotential) with quantum calculations for the Coulomb system is not expected for frequencies above the plasma frequency. In particular, the high-frequency asymptote is not correctly reproduced.

V. STATIC COLLISION FREQUENCY

Another important aspect is the validity range of perturbative results obtained by the quantum-statistical approach. As discussed above (see also [1]), perturbative analytical results are applicable in the region $\Gamma \leqslant 2$. For strongly coupled plasmas, interpolation formulas can be constructed based on correct analytical behavior in limiting cases and simulation data for intermediate regions. In the following, we will discuss the results from MD simulations, analytical approaches, and experimental data for the electrical conductivity in the static limit.

From MD simulations for the current ACF, we have calculated the collision frequency $\nu(\omega)$. According to relation (4), we obtain the dc conductivity $\sigma_{\rm dc} = \epsilon_0 \omega_{\rm pl}^2 / \nu(0)$. Results for $\nu(0)$ as a function of temperature at fixed nonideality parameter $\Gamma = 1$ are shown in Fig. 10. Apart from the parameter sets given in Table I, further simulations have been done. Simulations have also been performed for a fixed temperature of $T = 33\,000$ K and varying coupling parameter Γ. Results for the collision frequency and the static conductivity including error bars are shown in Figs. 11 and 12.

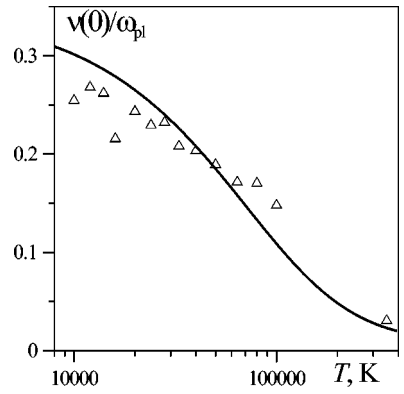

FIG. 10. Dependence of the static collision frequency on temperature at $\Gamma = 1$. Δ: MD results for the Kelbg potential (8). Solid line: interpolation formula (33).

The perturbative approach to the dynamic conductivity [5], mentioned above, has been extended for the static limit $\omega = 0$ to a larger region of plasma parameter values. In particular, an interpolation formula for the dc conductivity of a fully ionized Coulomb plasma was derived recently [37]. Using analytical results of the quantum-statistical approach for different limiting cases as an input, the following expression for the dc conductivity has been given as function of Γ and Θ:

$$\sigma_{\rm dc}^{\rm ERR} = a_0 T^{3/2} \left(1 + \frac{b_1}{\Theta^{3/2}}\right) \left[D \ln(1 + A + B) - C - \frac{b_2}{b_2 + \Gamma\Theta} \right]^{-1}, \tag{33}$$

where T in K, σ in $(\Omega\,\mathrm{m})^{-1}$, and with the functions

$$A = \Gamma^{-3} \frac{1 + a_4/\Gamma^2\Theta}{1 + a_2/\Gamma^2\Theta + a_3/\Gamma^4\Theta^2} [a_1 + c_1 \ln(c_2 \Gamma^{3/2} + 1)]^2,$$

$$B = b_3(1 + c_3\Theta)/\Gamma\Theta/(1 + c_3\Theta^{4/5}),$$

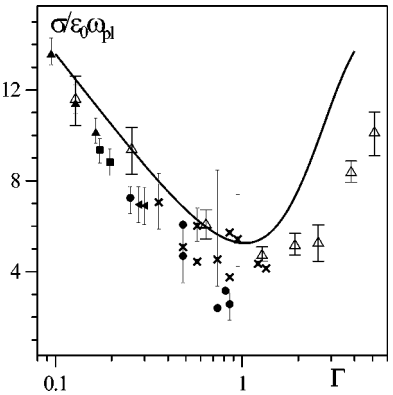

FIG. 11. Static conductivity depending on the nonideality parameter Γ. △: MD results for the Kelbg potential (8) for $T = 33\,000$ K. Solid line: interpolation formula (33) for $T = 33\,000$ K. Experimental data: ● [39], × [40], ■ [41], ▲ [42], and ◀ [43].

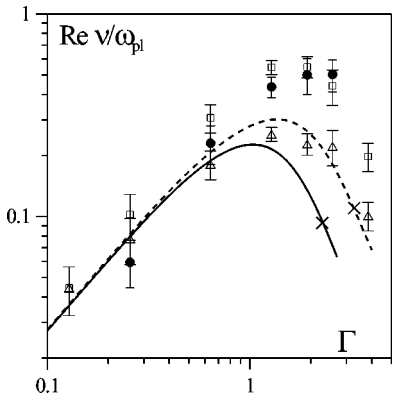

FIG. 12. Static and dynamic collision frequencies. MD results for the Kelbg potential (8). △: $\nu(\omega=0)$ obtained from current ACF. □: $\nu(\omega_{\rm pl})$ obtained from current ACF. ●: collisional damping of the Langmuir waves $\nu=2\delta_c$ [31]. Interpolation formula (33): Solid curve: $T=33\,000$ K. Dashed curve: $T=16\,000$ K. × correspond to $\Theta(n_e,T)=1$.

$$C = c_4/[\ln(1+\Gamma^{-1}) + c_5\Gamma^2\Theta],$$

$$D = [\Gamma^3 + a_5(1 + a_6\Gamma^{3/2})]/(\Gamma^3 + a_5).$$

The set of parameters is given by $a_0=0.030\,64$, $a_1=1.1590$, $a_2=0.698$, $a_3=0.4876$, $a_4=0.1748$, $a_5=0.1$, $a_6=0.258$, $b_1=1.95$, $b_2=2.88$, $b_3=3.6$, $c_1=1.5$, $c_2=6.2$, $c_3=0.3$, $c_4=0.35$, and $c_5=0.1$. They are fixed by the low-density expansion of the dc conductivity (Spitzer formula) (see below), the strong degenerate limit, and numerical data for the dc conductivity in the intermediate parameter region. This expression is an improvement of well-known approximations for the static conductivity such as the Born result

$$\sigma_{\rm dc}^{\rm Born} = 0.299\frac{(4\pi\epsilon_0)^2(k_{\rm B}T)^{3/2}}{e^2m^{1/2}}\left[\frac{1}{2}\ln\frac{\Theta}{\Gamma}\right]^{-1} \qquad (34)$$

for a statically screened Coulomb potential [38] or the Spitzer formula for the low-density limit:

$$\sigma_{\rm dc}^{\rm Spitzer} = 0.591\frac{(4\pi\epsilon_0)^2(k_{\rm B}T)^{3/2}}{e^2m^{1/2}}\left[-\frac{3}{2}\ln\Gamma\right]^{-1}. \qquad (35)$$

Considering the MD simulations for $\Gamma=1$, Fig. 10, the systematic behavior agrees very well with analytical results obtained from the interpolation formula (33).

With respect to the simulations of the dc conductivity for a fixed temperature $T=33\,000$ K and varying coupling parameter Γ shown in Fig. 11, comparison with the interpolation formula (33) and with experimental data is made. While the agreement between the simulation results and the interpolation formula is excellent for values up to $\Gamma=1$, discrepancies arise for higher values of Γ. However, the principal behavior of the MD simulations can be reproduced with the interpolation formula. In contrast, larger discrepancies are found when comparing results for finite frequencies; see Fig. 9. The theoretical description, based on analytical expressions and MD simulations, leads to a good understanding of experimental results which are shown in the figure as well.

A compilation of various results for the static and the dynamic collision frequencies is shown in Fig. 12. Besides the values for the real part of the collision frequency at $\omega=\omega_{\rm pl}$ as obtained from the current ACF, data for the collisional damping δ_c of the Langmuir waves at $k=0$ are shown. These were obtained in Ref. [31] through extrapolation of MD data for the total damping $\delta(k)$ to the limiting value at $k\to 0$. The data for $\delta(k)$ were found measuring the width of the peak of $S(k,\omega)$ which corresponds to the Langmuir waves. The interpolation procedure was based on the supposition that the Landau damping in a nonideal plasma does not differ significantly from that in the ideal plasma. This assumption was supported by MD results in [31]. Comments on the static results were already made in the context of Fig. 11 above. Regarding the dynamic results, a reasonable agreement is obtained between the different approaches. The larger values for the collision frequency at $\omega=\omega_{\rm pl}$ compared with the static values $\nu(0)$ have also been shown in Fig. 7 above.

VI. CONCLUSION

We discuss the optical conductivity of dense plasmas, considering experiment, theory, and numerical simulations as three different aspects. As a special case, the optical conductivity $\sigma(\omega)$ includes the dc conductivity $\sigma_{\rm dc}=\sigma(0)$.

Our focus is on MD simulations for the current ACF's. They are used to extract the dynamical conductivity $\sigma(\omega)$ as well as the dynamical collision frequency $\nu(\omega)$. Refined MD simulation procedures led to qualitative improvements in comparison to previous results in [12]. For the first time, we showed that after introducing a mean-field contribution, longitudinal and transverse conductivities coincide in the long-wavelength limit $k\to 0$ within the numerical accuracy. Various known properties such as the high-frequency behavior and analytic constraints like the Kramers-Kronig relations were used to assess the MD results and to show the consistency of our approach. For all conditions considered here, these restrictions were fulfilled within the numerical precision. Treating the mean field separately, the remaining contributions to the long-range part of the forces are accounted for by Ewald sums which give only a marginal effect if the simulation box is sufficiently large.

However, the classical MD simulations are based on a pseudopotential instead of the original Coulomb interaction. As an appropriate potential to mimic quantum effects, the Kelbg potential is taken which is obtained from a systematic treatment of quantum effects so that static equilibrium properties are correctly reproduced. It is an open question to which extent this potential is able to reproduce dynamic properties of a quantum Coulomb system. Further investigations will compare MD simulations with wave packet or path integral simulations which allow for a more consistent treatment of quantum effects. In particular, the formation of bound states will be an essential aspect in the future development of numerical simulations.

Theoretical investigations are based on quantum statistics, taking adequately into account the Coulomb interaction and quantum effects. In this approach, the formation of bound

states is correctly included. Present perturbative treatments lead to analytical results. However, they are restricted to small nonideality parameter values $\Gamma \leqslant 1$ or small plasma densities n. In our approach, the weak-coupling limit has been improved, taking into account dynamical screening and strong binary collisions. Considering a renormalization factor $r(\omega)$, the correct low-density limit of transport coefficients is achieved. The comparison with MD simulations shows that the low-frequency behavior of the optical conductivity is given in good approximation as long as $\Gamma \leqslant 1$. For higher values of Γ, the quantum-statistical approach has to be evaluated using methods beyond perturbation theory or by deriving interpolation formulas. On the other hand, MD simulations based on the Kelbg pseudopotential cannot reproduce the correct high-frequency ($\omega > \omega_{\mathrm{pl}}$) behavior of the optical conductivity for quantum Coulomb systems.

Within the quantum-statistical treatment, the formation of bound states is described in the low-density limit applying the model of a partially ionized plasma. At high densities, this model breaks down, and one has to apply adequate concepts such as the spectral function in order to describe the density modification due to medium effects, in particular the dissolution of bound states. This consideration of bound states becomes more involved if, instead of a simple hydrogen plasma, ions with higher charges are considered allowing for different stages of ionization.

MD simulations as well as quantum-statistical calculations of the dynamical conductivity have to be confronted with experimental data. In this paper we focused on the dc conductivity. For small nonideality up to $\Gamma \approx 1$, we found satisfactory coincidence between theory, MD simulations, and experiments. In forthcoming work, applications to bremsstrahlung [2] as well as Thomson scattering [44] should be analyzed in order to investigate the dynamical collision frequency at higher frequencies. As already discussed above, classical MD simulations based on pseudopotentials such as the Kelbg one fail to reproduce the correct high-frequency asymptote for the collision frequency so that larger discrepancies compared with experiments are expected. Instead of classical MD simulations, consistent quantum simulations such as wave-packet molecular dynamics or path integral techniques have to be used to compare with experimental data for high frequencies.

Experimental results suffer, e.g., from the transient nature of the produced plasma. Ionization, density, and temperature profiles have to be considered to infer local plasma conditions in order to compare with simulations or calculations. Experiments are performed not only with hydrogen plasmas, but also with other materials, in which case the electron interactions are not pure Coulomb anymore. The formation of bound states is an important feature in present experiments, since the contribution of the ionized component is extracted by applying the model of the partially ionized plasma. Nevertheless, for the plasma conditions considered here, the consistency between MD simulations, perturbative calculations, and experimental results is inferred from the present work.

ACKNOWLEDGMENTS

The authors thank R. Thiele and Th. Millat for some of the numerical calculations as well as G.E. Norman, and A.A. Valuev for fruitful discussions. I.M. acknowledges support from RFBS by Grant No. 03-07-90272v, the Dynasty Foundation, and the International Center of Fundamental Physics in Moscow. H.R. and G.R. acknowledge support through the Virtual Institute VI/VH 104 from the Helmholtz Gemeinschaft.

[1] A. Selchow, G. Röpke, A. Wierling, H. Reinholz, T. Pschiwul, and G. Zwicknagel, Phys. Rev. E **64**, 056410 (2001).
[2] A. Wierling, Th. Millat, G. Röpke, R. Redmer, and H. Reinholz, Phys. Plasmas **8**, 3810 (2001).
[3] A. Wierling, Th. Millat, and G. Röpke, J. Plasma Phys. **70**, 185 (2004).
[4] H. Reinholz, Yu. Zaporoghets, V. Mintsev, V. Fortov, I. Morozov, and G. Röpke, Phys. Rev. E **68**, 036403 (2003).
[5] H. Reinholz, R. Redmer, G. Röpke, and A. Wierling, Phys. Rev. E **62**, 5648 (2000).
[6] H. Reinholz, Aust. J. Phys. **53**, 133 (2000).
[7] H. Reinholz, G. Röpke, I. Morozov, V. Mintsev, Yu. Zaparoghets, V. Fortov, and A. Wierling, J. Phys. A **36**, 5991 (2003).
[8] V. P. Silin, Zh. Eksp. Teor. Fiz. **47**, 2254 (1964) [Sov. Phys. JETP **20**, 1510 (1965)].
[9] C. D. Decker, W. B. Mori, J. M. Dawson, and T. Katsouleas, Phys. Plasmas **1**, 4043 (1994).
[10] P. Mulser, F. Cornolti, E. Bésuelle, and R. Schneider, Phys. Rev. E **63**, 016406 (2000).
[11] Th. Bornath, M. Schlanges, P. Hilse, and D. Kremp, Phys. Rev. E **64**, 026414 (2001).
[12] H. Reinholz, I. Morozov, G. Röpke and Th. Millat, Phys. Rev. E **69**, 066412 (2004).
[13] J. P. Hansen, and I. R. McDonald, Phys. Rev. A **23**, 2041 (1981); L. Sjögren, J. P. Hansen, and E. L. Pollock, *ibid.* **24**, 1544 (1981).
[14] J. P. Hansen and I. R. McDonald, *Theory of Simple Liquids* (Academic Press, London, 1976).
[15] J. P. Hansen, in *Strongly Coupled Plasma Physics*, edited by F. J. Rogers, H. E. DeWitt (Plenum, New York, 1987), p. 111.
[16] I. V. Morozov, G. E. Norman, and A. A. Valuev, Dokl. Akad. Nauk **362**, 752 (1998) Dokl. Phys. **43**, 608 (1998).
[17] I. V. Morozov, G. E. Norman, and A. A. Valuev, Phys. Rev. E **63**, 036405 (2001).
[18] D. Klakow, C. Toepffer, and P.-G. Reinhard, J. Chem. Phys. **101**, 10766 (1994); M. Knaup, P.-G. Reinhard, and C. Toepffer, Contrib. Plasma Phys. **41**, 159 (2001).
[19] B. Militzer and D. M. Ceperley, Phys. Rev. Lett. **85**, 1890 (2000).
[20] W.-D. Kraeft, D. Kremp, W. Ebeling, and G. Röpke, *Quantum Statistics of Charged Particle Systems* (Plenum, New York, 1986).
[21] C. Deutsch, Phys. Lett. **60A**, 317 (1977); C. Deutsch, M. M.

Combert, and H. Minoo, *ibid.* **66A**, 381 (1978).
[22] T. Pschiwul and G. Zwicknagel, J. Phys. A **36**, 6251 (2003).
[23] T. Pschiwul and G. Zwicknagel, Contrib. Plasma Phys. **43**, 393 (2003).
[24] W. Ebeling, G. E. Norman, A. A. Valuev, and I. A. Valuev, Contrib. Plasma Phys. **39**, 61 (1999).
[25] A. V. Filinov, M. Bonitz, and W. Ebeling, J. Phys. A **36**, 5957 (2003).
[26] G. D. Mahan, *Many-Particle Physics* (Plenum, New York, 1990).
[27] S. Ichimaru, Vol. 1, *Statistical Plasma Physics: Basic Principles*, (Addison-Wesley, Reading, MA, 1992).
[28] R. Kubo, M. Toda, and N. Hashitsume, *Statistical Physics II* (Springer, Berlin, 1985).
[29] We stress that linear response is not applicable in strong fields-e.g., in intense laser beams; see [9-11].
[30] M. P. Allen and D. J. Tildesley, *Computer Simulation of Liquids* (Clarendon Press, Oxford, 1987).
[31] I. V. Morozov and G. E. Norman, JETP **100**, 370 (2005).
[32] Th. Millat, PhD thesis, University of Rostock, 2003.
[33] Th. Millat, A. Selchow, A. Wierling, H. Reinholz, R. Redmer, and G. Röpke, J. Phys. A **36**, 6259 (2003).
[34] S. Pfalzner and P. Gibbon, Phys. Rev. E **57**, 4698 (1998).
[35] M. Schlanges, Th. Bornath, D. Kremp and P. Hilse, Contrib. Plasma Phys. **43**, 360 (2003).
[36] Th. Bornath, M. Schlanges, P. Hilse, and D. Kremp, J. Phys. A **36**, 5941 (2003).
[37] A. Esser, R. Redmer, and G. Röpke, Contrib. Plasma Phys. **43**, 33 (2003).
[38] J. M. Ziman, Philos. Mag. **6**, 1013 (1961).
[39] V. A. Sechenov, E. E. Son, and O. E. Shchekotov, Sov. Phys. TVT **15**, 415 (1977).
[40] Yu. V. Ivanov, V. B. Mintsev, V. E. Fortov, and A. N. Dremin, Sov. Phys. JETP **71**, 216 (1976).
[41] A. A. Bakeev and R. E. Rovinskii, Sov. Phys. TVT **8**, 1121 (1970).
[42] V. M. Batenin and P. V. Minaev, Sov. Phys. TVT **9**, 676 (1971).
[43] S. I. Andreev and T. V. Gavrilova, Sov. Phys. TVT **13**, 176 (1975).
[44] A. Höll, R. Redmer, G. Röpke, and H. Reinholz, Eur. Phys. J. D **29**, 159 (2004); IEEE Trans. Plasma Sci. **33**, 77 (2005).